Human Cell (2019) 32:51–63
https://doi.org/10.1007/s13577-018-0222-1

RESEARCH ARTICLE

Human amniotic fluid stem cells have a unique potential to accelerate cutaneous wound healing with reduced fibrotic scarring like a fetus

Marie Fukutake[1] · Daigo Ochiai[1] · Hirotaka Masuda[1] · Yushi Abe[1] · Yu Sato[1] · Toshimitsu Otani[1] · Shigeki Sakai[3] · Noriko Aramaki-Hattori[3] · Masayuki Shimoda[2] · Tadashi Matsumoto[1] · Kei Miyakoshi[1] · Yae Kanai[2] · Kazuo Kishi[3] · Mamoru Tanaka[1]

Received: 31 July 2018 / Accepted: 8 November 2018 / Published online: 1 December 2018

Abstract

Adult wound healing can result in fibrotic scarring (FS) characterized by excess expression of myofibroblasts and increased type I/type III collagen expression. In contrast, fetal wound healing results in complete regeneration without FS, and the mechanism remains unclear. Amniotic fluid cells could contribute to scar-free wound healing, but the effects of human amniotic fluid cells are not well characterized. Here, we determined the effect of human amniotic fluid stem cells (hAFS) on FS during wound healing. Human amniotic fluid was obtained by amniocentesis at 15–17 weeks of gestation. CD117-positive cells were isolated and defined as hAFS. hAFS (1×10^6) suspended in PBS or cell-free PBS were injected around wounds created in the dorsal region of BALB/c mice. Wound size was macroscopically measured, and re-epithelialization in the epidermis, granulation tissue area in the dermis and collagen contents in the regenerated wound were histologically analyzed. The ability of hAFS to engraft in the wound was assessed by tracking hAFS labeled with PKH-26. hAFS fulfilled the minimal criteria for mesenchymal stem cells. hAFS injection into the wound accelerated wound closure via enhancement of re-epithelialization with less FS. The process was characterized by lower numbers of myofibroblasts and higher expression of type III collagen. Finally, transplanted hAFS were clearly observed in the dermis until day 7 implying that hAFS worked in a paracrine manner. hAFS can function in a paracrine manner to accelerate cutaneous wound healing, producing less FS, a process resembling fetal wound healing.

Keywords Human amniotic fluid stem cell · Wound healing · Epithelialization · Fibrosis · Scar formation

Introduction

Cutaneous wound healing is a complex process that involves inflammation, cell proliferation, differentiation, migration, angiogenesis and remodeling of the extracellular matrix (ECM) [1]. It requires the cooperation of multiple cell types, cytokines and ECM proteins. There are phenotypic differences between the collagen components in fetal and adult wounds [2–6]. In adults, it sometimes results in a non-functional mass of fibrotic tissue at the site of the regenerated tissue (a scar), characterized by abnormal ECM remodeling such as excessive deposition of type I collagen [7]. In contrast, fetal wound healing results in complete regeneration without fibrotic scarring, characterized by rapid deposition of type III collagen in a fine reticular network [2–6]. The factors responsible for scarless fetal wound healing have been attributed to intrinsic factors in the developing fetal dermis secondary to gene expression associated with the

Electronic supplementary material The online version of this article (https://doi.org/10.1007/s13577-018-0222-1) contains supplementary material, which is available to authorized users.

✉ Daigo Ochiai
ochiaidaigo@keio.jp

[1] Department of Obstetrics and Gynecology, Keio University School of Medicine, 35, Shinanomachi Shinjyukuku, Tokyo 160-8582, Japan

[2] Department of Pathology, Keio University School of Medicine, 35, Shinanomachi Shinjyukuku, Tokyo 160-8582, Japan

[3] Department of Plastic and Reconstructive Surgery, Keio University School of Medicine, 35, Shinanomachi Shinjyukuku, Tokyo 160-8582, Japan

development of fetal skin [2, 3]. However, the extrinsic factors responsible for scar-free fetal wound healing remain to be determined. Significantly, several studies suggested that the extrinsic factors in amniotic fluid and/or amniotic fluid cells contribute to scarless fetal wound healing [3, 8].

Mesenchymal stem cells (MSCs) are emerging as a promising cell population for the promotion of wound healing and their therapeutic potential depends on the origin of the MSC [9–11]. Among the different sources of MSCs, those derived from amniotic fluid have a number of characteristics that make them attractive candidates for stem cell therapy for neonates [12, 13]. Amniotic cells can be easily collected during routine prenatal testing and could be saved for future stem cell therapy, as needed. Amniotic cells are not subject to ethical debates because the residual amniotic fluid remaining after genetic research is normally destroyed [12–14]. However, few studies have focused on the therapeutic effects of human amniotic fluid stem cells (hAFS) on wound healing, especially on ECM remodeling.

The aim of this study was to determine the effect of hAFS on fibrotic scarring during wound healing. Towards that end, we injected hAFS around a dorsal lesion in BALB/c mice and evaluated ECM remodeling in the regenerated tissue during wound healing.

Materials and methods

Isolation and culture of CD117$^+$ amniotic fluid cells

The study was approved by the institutional review board of Keio University School of Medicine (No. 20140285) and informed consent was obtained from all patients in writing. Patients were all adults. Five-milliliter samples of amniotic fluid were obtained from pregnant women who underwent amniocentesis at 15–17 weeks of gestation. Within 2 h, amniotic fluid samples were centrifuged at 1500 rpm for 5 min. After removal of the supernatant, the cells were cultured at 37 °C in a humidified incubator containing 5% CO_2. Amniotic fluid cell culture medium was composed of minimum essential medium (a-MEM; Gibco, Langley, OK, USA) supplemented with 20% Chang Medium (18% Chang B plus 2%Chang C; Irvine Scientific, Santa Ana, CA, USA), fetal bovine serum (FBS) (BioWest, Miami, FL, USA), 1% glutamine (GIBCO) and 1% penicillin/streptomycin (Wako Pure Chemical, Osaka, Japan). For further selection of stem cell populations, growth medium was replaced every 4 days until the cell population became sub-confluent. Subsequently, CD117-positive (CD 117$^+$) cells were isolated by a magnetic cell-sorting kit (Miltenyi Biotec, Auburn, CA, USA), as previously reported [12]. CD117$^+$ cells were plated and expanded to higher passages for further analysis.

Immunophenotypic analysis of CD117$^+$ amniotic fluid cells

CD117$^+$ cells were characterized by flow cytometry for surface markers of mesenchymal (CD29, CD73, and CD90) and hematopoietic (CD14, CD34, and HLA-DR) stem cells. A total of 1×10^5 cells were harvested and incubated with either PE, FITC or APC-conjugated antibodies against CD29, CD73, CD90, CD14, CD34, and HLA-DR mouse anti-human monoclonal antibodies and appropriate isotype controls. Stained cells were then analyzed using a MoFlo XDP flow cytometer (Beckman Coulter, Inc., Brea, CA, USA) using Cell Quest software, and data were analyzed using Summit software. Antibody information is listed in Table 1.

Analysis of the differentiation potential of CD117$^+$ amniotic fluid cells

To investigate the differentiation capacity of hAFS, CD117$^+$ cells were differentiated in vitro into osteogenic, adipogenic, chondrogenic, neurogenic and cardiomyogenic lineages. CD117$^+$ cells were cultured in expansion medium until 70% confluence was reached. The culture was then shifted to a specific induction medium at 37 °C in a humidified incubator containing 5% CO_2. Thus, CD117$^+$ cells were cultured in 'adipogenic differentiation medium', 'osteogenic differentiation medium' (Lonza, Basel, Switzerland), 'neurogenic differentiation medium' (PromoCell GmbH, Heidelberg, Germany) or 'cardiomyogenic differentiation medium' (Cellular Engineering Technologies, Inc., Iowa, USA) for the appropriate time according to the manufacturer's recommended protocol. To induce chondrogenic differentiation, a total of

Table 1 List of antibodies used for flow cytometric analysis in this study

Antigen	Clone	Concentration	Source of reference
CD14	TUK4	10 µl/2.5 × 10^5 cell	Miltenyi Biotec, Auburn, CA, USA
CD29	AG89	20 µl/2.5 × 10^5 cell	MBL CO., LTD., Nagoya, Japan
CD34	581	20 µl/2.5 × 10^5 cell	BD Bioscience Pharmingen, San Diego, CA, USA
CD73	AD2	20 µl/2.5 × 10^5 cell	BioLegend Inc., San Diego, CA, USA
CD90	5E10	20 µl/2.5 × 10^5 cell	BioLegend Inc., San Diego, CA, USA
HLA-DR	B8.12.2	20 µl/2.5 × 10^5 cell	Beckman Coulter, Inc., Brea, CA, USA

2.5×10^5 cells were placed into a 15-mL conical polypropylene tube and centrifuged at 1500 rpm for 10 min. Then cell pellets (1 pellet/tube) were cultured for 21 days in 'chondrogenic differentiation medium' (Lonza, Basel, Switzerland).

Osteogenesis was assessed by Alizarin staining (Cosmo Bio Co., Ltd. Tokyo, Japan) of the calcified extracellular matrix deposition. Oil red O staining was used for detection of intracellular lipid droplet formation to evaluate adipogenesis. Chondrogenic differentiation was determined by Alcian Blue staining. For the evaluation of neural differentiation, we immunostained cells for the neuron-specific marker MAP-2. Differentiation into the cardiomyogenic lineage was determined by cardiac troponin T immunostaining. Antibody information is listed in Table 2.

Enzyme-linked immunosorbent assay (ELISA) of paracrine mediators secreted from hAFS

hAFS at passages 4–6 were seeded on 35-mm culture dishes with amniotic fluid cell culture medium at a density of 1×10^5 cells/well. After 72 h, the confluent cells were washed with PBS and then incubated in amniotic fluid cell culture medium. After another 12 h, 24 h, 48 h and 72 h, the medium was collected and designated "conditioned medium derived from hAFS". Paracrine mediator levels for vascular endothelial growth factor (VEGF), IL-10 and PGE_2 were determined using ELISA kits according to the manufacturer's protocol.

A dorsal excisional cutaneous wound model in BALB/c mice

BALB/c mice (8 weeks old; male; body weight, 20–23 g) were obtained from Oriental Yeast Co., Ltd. (OYC, Tokyo, Japan). To prepare skin defects, mice were anesthetized with 3% isoflurane followed by maintenance with 2% isoflurane. After hair removal from the dorsal surface, 8-mm full-thickness excisional skin wounds were created on each side of the midline using a sterile biopsy punch (Kai Industries Co., Ltd, Japan). We injected 240 µL PBS (containing or lacking 1×10^6 hAFS) around the wound at 6 injection sites. Wounds were then covered with an occlusive dressing (Tegaderm, Sumitomo 3M, Ltd., Tokyo, Japan) and an elastic adhesive bandage (Silkytex, ALCARE Co, Ltd., Tokyo, Japan). All procedures were performed according to the guidelines for the Care and Use of Laboratory Animals of Keio University School of Medicine, and were approved by the Animal Study Committee of Keio University (IRB approval number 15083-(0)).

Macroscopic and histological analyses of cutaneous wounds

Mice were killed by atlantoaxial subluxation, and skin with the wound was removed. Wound size was macroscopically monitored with a microscope camera (Leica, Wetzlar, Germany) 0, 7, 14 and 21 days after the treatment. Wound sizes (percentage of wound area to initial wound area) were calculated from the photographs using ImageJ software (http://www.rsb.info.nih.gov/ij; $n = 5$ per group).

Skin samples were harvested 0, 7, 14, and 21 days after the treatment. Excised specimens were fixed with 4% paraformaldehyde for paraffin embedding. Paraffin sections (4 µm) were treated with H&E, Masson's Trichrome, Elastica van Gieson and Picrosirius red stains. Immunostaining for α-smooth muscle actin (α-SMA), type I and III collagen was also performed. Antibody information is listed in Table 2. Stained sections were viewed by microscopy (BZ-9000, KEYENCE, Osaka, Japan), and Picrosirius

Table 2 List of antibodies used for immunofluorescence staining in this study

Primary antibody	Clone	Concentration	Source of reference
MAP-2	Mouse IgGl	1:100	Sigma-Aldrich, St. Louis, MO, USA
Cardiac troponin T	Mouse IgGl	1:100	Thermo Fisher Scientific, Waltham, MA, USA
Smooth muscle actin	1A4	1:200	Dako, Carpinteria, CA, USA
Collagen I	Rabbit polyclonal	1:200	Abeam, Cambridge, UK
Collagen III	Rabbit polyclonal	1:1000	Abeam, Cambridge, UK

Secondary antibody	Concentration	Source of reference
Goat anti-rabbit IgG Alexa four 488	1:250	Thermo Fisher Scientific, Waltham, MA, USA
Goat anti-mouse IgM Alexa four 488	1:250	Thermo Fisher Scientific, Waltham, MA, USA
Goat anti-mouse IgG Alexa four 555	1:250	Thermo Fisher Scientific, Waltham, MA, USA

red-stained sections were observed using polarized microscopy (BX53-P, Olympus, Tokyo, Japan).

Morphometric analysis of re-epithelialization and formation of granulation tissue and myofibroblasts

The width of the wound and the distance of the traversed epithelium were measured on Masson's Trichrome-stained sections, and the percentage of the tissue that underwent re-epithelialization was calculated according to the following formula: [distance covered by epithelium]/[distance across wound bed] × 100 ($n = 5$) [15]. The granulation tissue area in the wounds was determined on Elastica van Gieson-stained sections according to previous methods ($n = 5$) [15]. Myofibroblasts were identified by α-SMA immunostaining, a classical myofibroblast-specific method.

Assessment of the ability of hAFS to engraft in wound

hAFS were labeled with PKH-26 Red fluorescent cell linker kit, as per the manufacturer's protocol (Sigma-Aldrich, St. Louis, MO, USA). Cells (1×10^6) were seeded on 35-mm culture dishes with serum-free α-MEM. After 24 h, the cells were viewed by fluorescent microscopy (BZ-9000, KEYENCE). hAFS labeled with PKH-26 were injected around the wound at six injection sites. Each wound received 1×10^6 cells (hAFS labeled with PKH-26) suspended in 240 µL PBS or 240 µL cell-free PBS. Skin samples were harvested 1, 4, 7, 14 and 21 days after the treatment. Cryosections were stained with Hoechst-33342. Fluorescent images were captured using a fluorescent microscopy (BZ-9000, KEYENCE).

RNA isolation and quantitative real-time RT-PCR

Total RNA was isolated with an RNeasy mini kit (Qiagen, Hilden, Germany) according to the manufacturer's instruction. The total skin RNA underwent reverse transcription to cDNA using a Prime Script RT Master Mix (Takara Bio, Shiga, Japan). Quantitative PCRs were performed in duplicate in a volume of 25 µL per reaction in a 96-well Bio-Rad CFX96 Real-time PCR System (Bio-Rad, Inc., Hercules, CA, USA). Reaction mixtures included 5 ng of genomic DNA as template, 0.4 mM each primer (Thermo Fisher Scientific Inc., Tokyo, Japan), SYBR Premix Ex Taq II (Tli RNaseH Plus) (Takara Bio, Shiga, Japan), and sterile H_2O. The primer sets are listed in Table 3. PCR was performed as follows: pre-denaturation at 95 °C for 30 s, 45 cycles of denaturation at 95 °C for 5 s, annealing at 60 °C for 20 s. The negative control (without reverse transcriptase) had no signal. The relative level of gene expression for each sample was calculated using the $2^{-\Delta\Delta CT}$ method. Gene expression levels were normalized to that of *Gapdh* as an internal control.

Statistical analysis

All results are expressed as means ± SD. The quantitative variable was statistically analyzed using a one-way ANOVA followed by a Student's *t* test. $P < 0.05$ was considered statistically significant. Each analysis was performed with commercially available software (IBM SPSS Statistics 24).

Results

Isolation, culture and immunophenotypic characterization of CD117$^+$ amniotic fluid cells

Isolated amniotic fluid cells consisted of a mixed population of adherent cells with different morphologies and sizes. Most were spindle and round-shaped cells. After immunoselection and passage in culture, clonal spindle-shaped cells were expanded as stable lines (Fig. 1a). The cell-surface antigenic expression of CD117$^+$ amniotic fluid cells was determined flow cytometrically. CD117$^+$ amniotic fluid cells were strongly positive for mesenchymal markers, such as CD29, CD73, and CD90, whereas they were negative for hematopoietic markers such as CD14, CD34, and HLA-DR (Fig. 1b). We also determined the differentiation capability

Table 3 List of primer sequence used in this study

Gene name	Amplicon length (bp)	Forward primer sequences (5′–3′)	Reverse primer sequences (5′–3′)
Collagen, type I. alpha 1 (*Col1a1*)	145	ACTGGTACATCAGCCCGAACC	GACATTAGGCGCAGGAAGGTC
Collagen, type I, alpha 2 (*Col1a2*)	147	CAGGCCCAACCTGTAAACACC	CTGAGTTGCCATTTCCTTGGAG
Collagen, type III, alpha 1 (*Col3a1*)	170	CCATGACTGTCCCACGTAAGC	CCGGCTGGAAAGAAGTCTGAG
α-Smooth muscle actin (*Acta2*)	156	CAGGCATGGATGGCATCAATCAC	ACTCTAGCTGTGAAGTCAGTGTCG
Glyceraldehyde-3-phosphate dehydrogenase (*Gapdh*)	87	TGCACCACCAACTGCTTAGC	GGCATGGACTGTGGTCATGAG

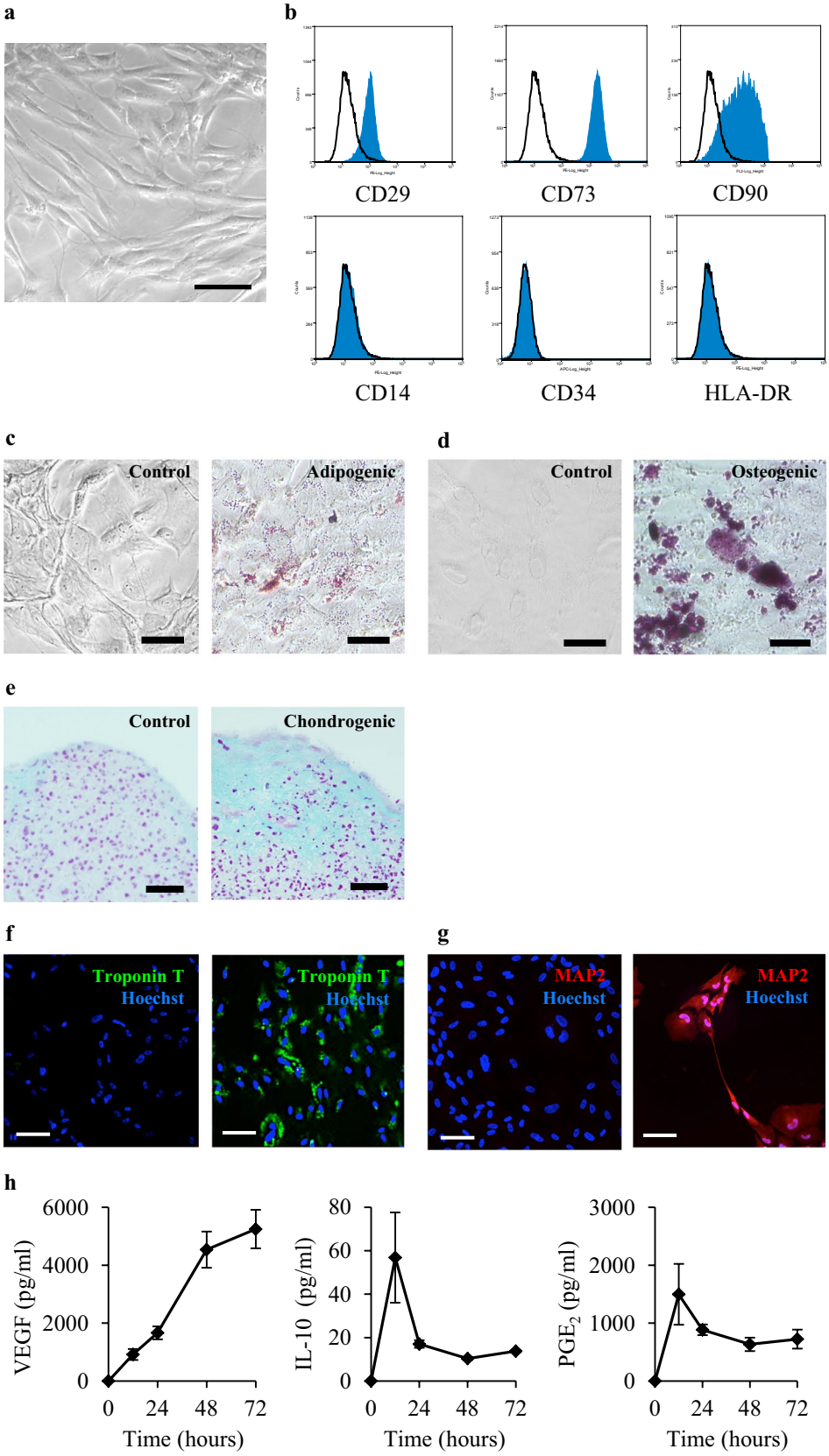

Fig. 1 Isolation, culture, and immunophenotypic characterization of CD117$^+$ amniotic fluid cells. **a** A bright-field image shows the morphology of CD117$^+$ amniotic fluid cells in culture. Scale bar = 100 µm. **b** CD117$^+$ amniotic fluid cells were stained with antibodies and analyzed by flow cytometry. **c**–**e** Representative microscopic images of CD117$^+$ amniotic fluid cells. The cells were cultured with adipogenic, osteogenic or chondrogenic differentiation media for appropriate times, and they were assessed by Oil red O (**c**), Alizarin red (**d**) or Alcian blue (**e**) staining. Scale bar = 50 µm. **f** Cardiomyogenic lineage-specific signals observed after cardiac troponin T staining. **g** Neuron lineage-specific signals exhibited after MAP-2 staining. **h** ELISA analysis of paracrine mediators secreted from CD117$^+$ amniotic fluid cells. Images are representative of 3 independent experiments performed with cells from different donors

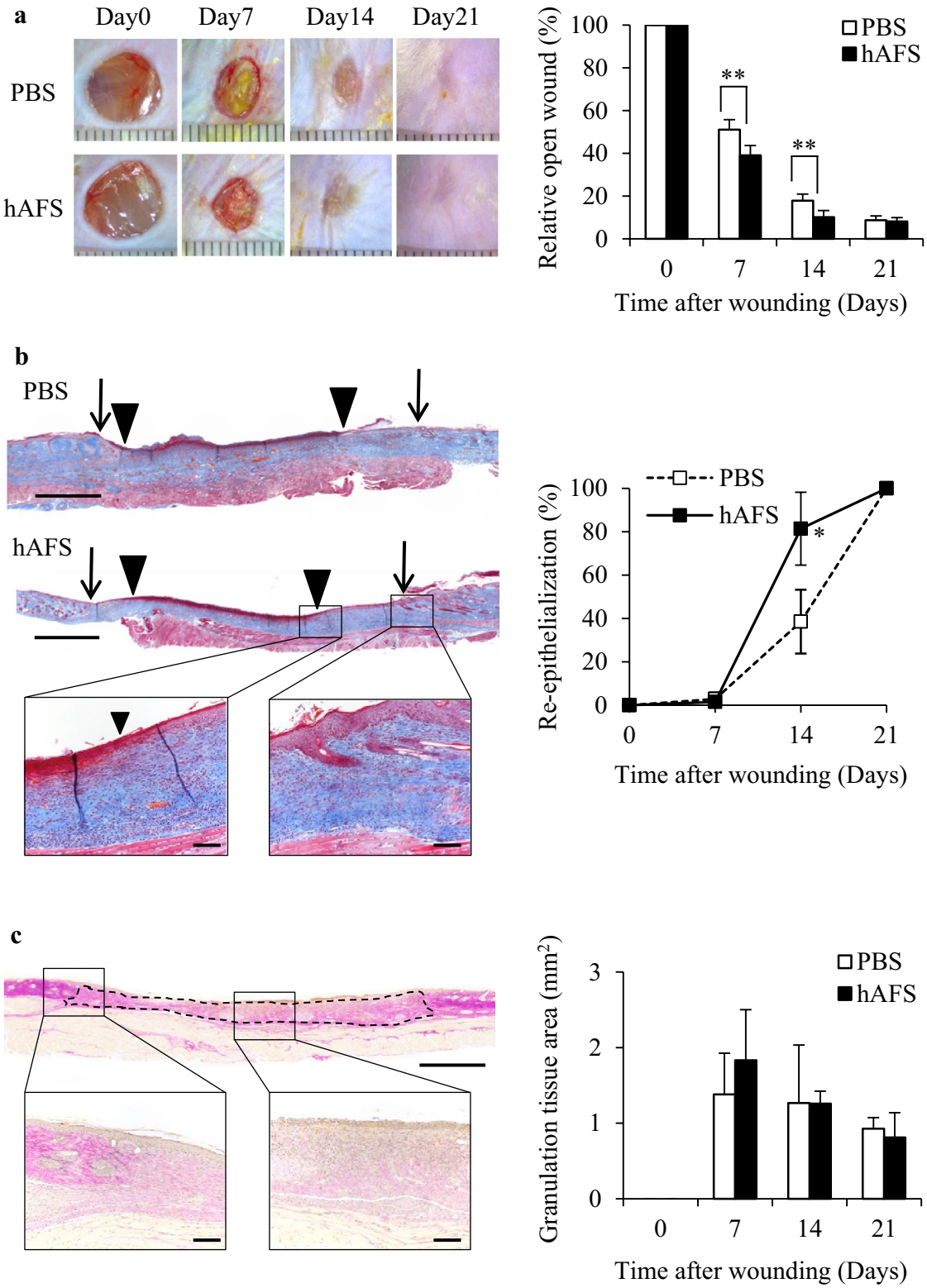

of CD117$^+$ amniotic fluid cells. These cells could differentiate towards adipogenic, osteogenic and chondrogenic lineages, as shown by Oil red O, Alizarin red, and Alcian blue staining, respectively (Fig. 1c–e). We evaluated the differentiation potential toward neuronal lineages and cardiomyogenic lineages. As expected, we observed the presence of cells that expressed MAP-2 as a neuronal marker (Fig. 1f) and cardiac troponin T as a cardiomyogenic marker

◂**Fig. 2** hAFS treatment enhanced cutaneous wound closure by accelerating re-epithelialization without affecting granulation tissue. **a** Representative images of full-thickness excisional wounds treated with phosphate-buffered saline (PBS), or 1.0×10^6 hAFS 0, 7, 14 and 21 days after the treatment (left). Data expressed as the percentage of the initial wound size at day 0 (right). **b** Representative images of Masson's Trichrome staining section 14 days after the treatment [wound margin (arrows) and the leading edge of the epithelia (arrowheads)] ($n=5$). The percentage of re-epithelialization was calculated according to the following formula: [distance covered by epithelium: distance between wound margin (arrow) − distance between the leading edge of epithelia (arrowheads)]/[distance between wound margin (arrow)]×100. Scale bar = 500 μm (upper), 100 μm (lower). **c** Representative images of Elastica van Gieson-stained sections 14 days after hAFS treatment. Dotted line shows the granulation tissue area. Quantification of granulation tissue areas after 0, 7, 14 and 21 days by the morphometric evaluation of granulation tissue area measured on Elastica van Gieson-stained sections ($n=5$). Scale bar = 500 μm (upper), 100 μm (lower). Results are presented as mean ± SD. $^*P<0.05$ and $^{**}P<0.01$ compared to control

(Fig. 1g). Based on these results, $CD117^+$ amniotic fluid cells were shown to fulfill the minimal criteria of an MSC population [16] with potentials for neuronal and cardiomyogenic differentiation, as previously reported [12, 13, 17, 18].

Paracrine mediators secreted from hAFS

To determine the molecular mediators secreted from hAFS, we used ELISA assays to examine conditioned medium derived from hAFS. ELISAs showed that VEGF levels gradually increased during the observation period, whereas IL-10 and PGE_2 levels peaked at 12 h and declined to baseline (Fig. 1h).

hAFS treatment transiently accelerated cutaneous wound closure by enhancing re-epithelialization of the epidermis without affecting the granulation tissue area in the dermis

To investigate whether hAFS treatment affected wound healing, we injected hAFS or PBS (control) around 8-mm full-thickness excisional skin wounds created on the backs of BALB/c mice. Macroscopic measurement of wound size demonstrated that hAFS treatment significantly accelerated wound closure compared to control (Fig. 2a). Acceleration of wound closure in hAFS groups was observed up to day 14, but there was no obvious difference between the 2 groups at day 21 (Fig. 2a). Additionally, an analysis of re-epithelialization in the epidermis measured on Masson's Trichrome-stained sections demonstrated that hAFS treatment significantly enhanced re-epithelialization after 14 days of treatment compared to control (Fig. 2b). Nevertheless, the granulation tissue area in the dermis measured on Elastica van Gieson-stained sections did not show any difference between the 2 groups during the observation period (Fig. 2c). These results indicated that hAFS treatment accelerated cutaneous wound closure by enhancing re-epithelialization in the epidermis without affecting the granulation tissue area in the dermis compared to controls.

hAFS decreased α-SMA expression in regenerated dermal tissues

In mice, the skin contraction induced by α-SMA-positive myofibroblasts as well as skin tissue generation contributes to cutaneous wound closure [1, 19]. To investigate whether skin contraction affected wound closure, we evaluated α-SMA-positive cells in granulation tissue. We found that hAFS significantly decreased α-SMA-positive expression by myofibroblasts compared to controls (Fig. 3a, b). In addition, quantitative real-time PCR analysis also showed a significant reduction in mRNA levels of α-SMA at day 14 in the hAFS group compared to controls (Fig. 3c). These observations suggested that hAFS regulated the rate of fibroblast differentiation into α-SMA-positive myofibroblasts at the transcriptional level. Taken together, we confirmed that hAFS injection accelerated cutaneous wound closure independently of wound contraction.

hAFS treatment attenuated fibrotic changes in the regenerated wound

Myofibroblasts containing α-SMA protein play a central role in synthesizing fibrotic tissue containing excess type I collagen [1, 19]. Fibrotic scarring is the final consequence of wound healing and determines its quality. To investigate fibrotic scarring of the regenerated wound, we histologically examined collagen organization in regenerated wounds at day 21. Picrosirius red staining showed that type I collagen (red and yellow) bundle organization was markedly reduced and type III collagen (green) was increased in hAFS groups (Fig. 4a). As the ratio between type I collagen and type III collagen protein expression during wound healing represents a valuable indicator for tissue fibrosis [2, 5], we investigated type I and type III collagen expression in regenerated wounds at day 21. Although type I collagen expression was comparable between the 2 groups, type III collagen protein expression was markedly increased in hAFS groups compared to control (Fig. 4b). Furthermore, quantitative real-time PCR analysis showed an increase in mRNA levels for type III collagen during the observation period (Fig. 4c). There was an especially significant increase at day 14 in the hAFS group, although mRNA levels for type I collagen were comparable between the 2 groups except for a significant decrease *Col1a1* at day 7 in the hAFS group (Fig. 4c). These findings suggested that hAFS treatment exerted antifibrotic effects resembling fetal wound healing, which were

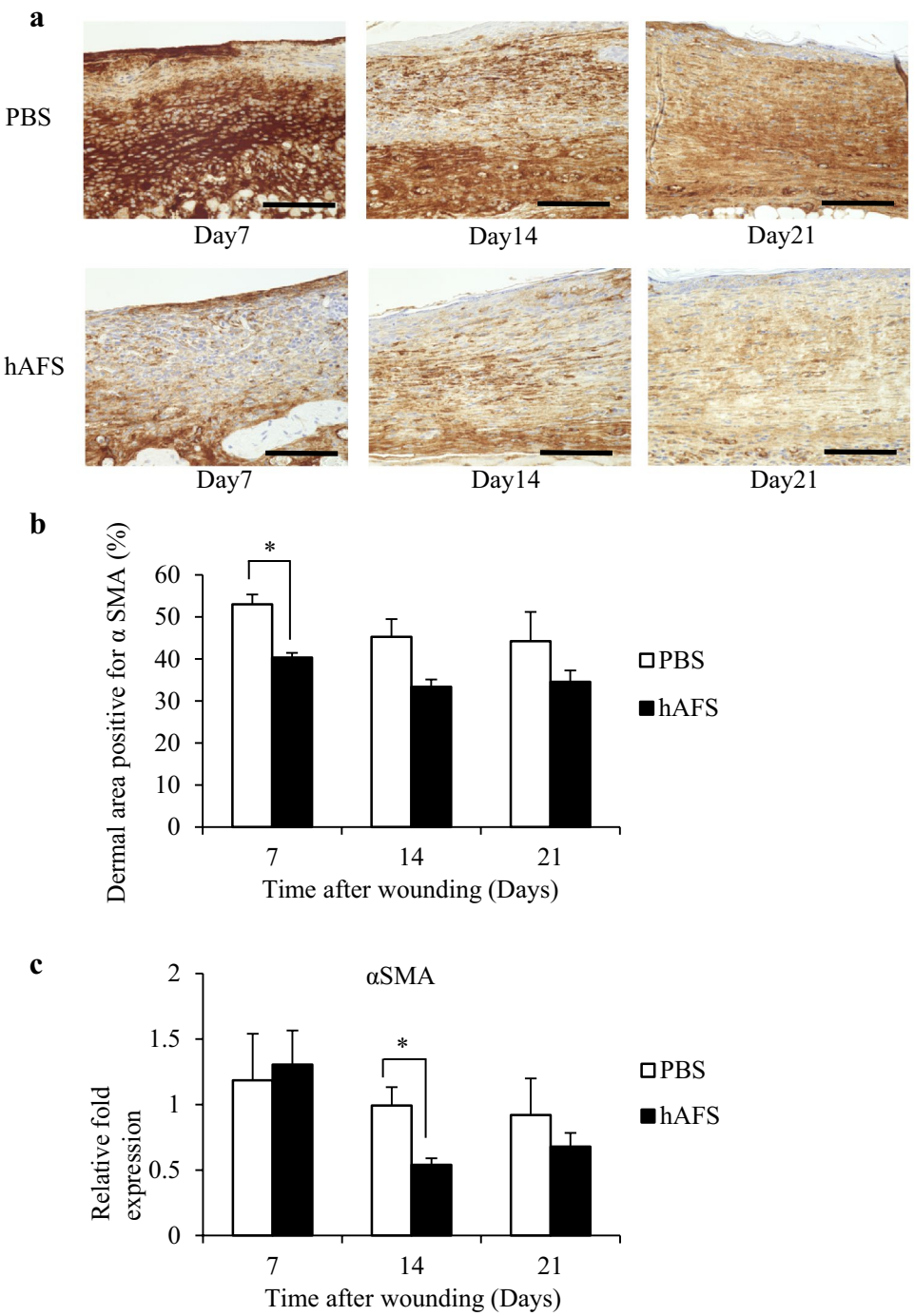

Fig. 3 hAFS treatment inhibited α-SMA-positive myofibroblast formation. **a** Representative images of treated regenerated wounds using antibodies against myofibroblast-specific marker α-SMA on days 7, 14 and 21. Scale bar = 500 µm. **b** Morphometric analysis of the α-SMA-positive area. Results are presented as means ± SD ($n = 3$). *$P < 0.05$ compared to control. **c** Quantitative real-time PCR of α-SMA expression levels on days 7, 14 and 21 ($n = 3$). Results are presented as means ± SD. *$P < 0.05$ compared to control

characterized by higher type III collagen expression regulated at the transcriptional level.

hAFS transiently engrafted in the wound

The ability of hAFS to engraft in a wound was assessed by hAFS labeled with PKH-26. We confirmed that hAFS could be labeled with PKH-26 in vitro by mixing cells with PKH-26 on culture dishes followed by 24-h cultivation. The cells were then assayed by fluorescent microscopy. This study clearly demonstrated that hAFS could be labeled with PKH-26 (Fig. 5a). To investigate the ability of hAFS to engraft in the wound, skin samples harvested after injection of hAFS labeled with PKH-26 were examined. At day 1 and day 4, large numbers of hAFS were observed both in the epidermis and dermis. However, after day 7, hAFS were mainly observed in the epidermis but not the dermis. At day 21, no labeled cells could be detected in the wound (Fig. 5b). Moreover, we also performed

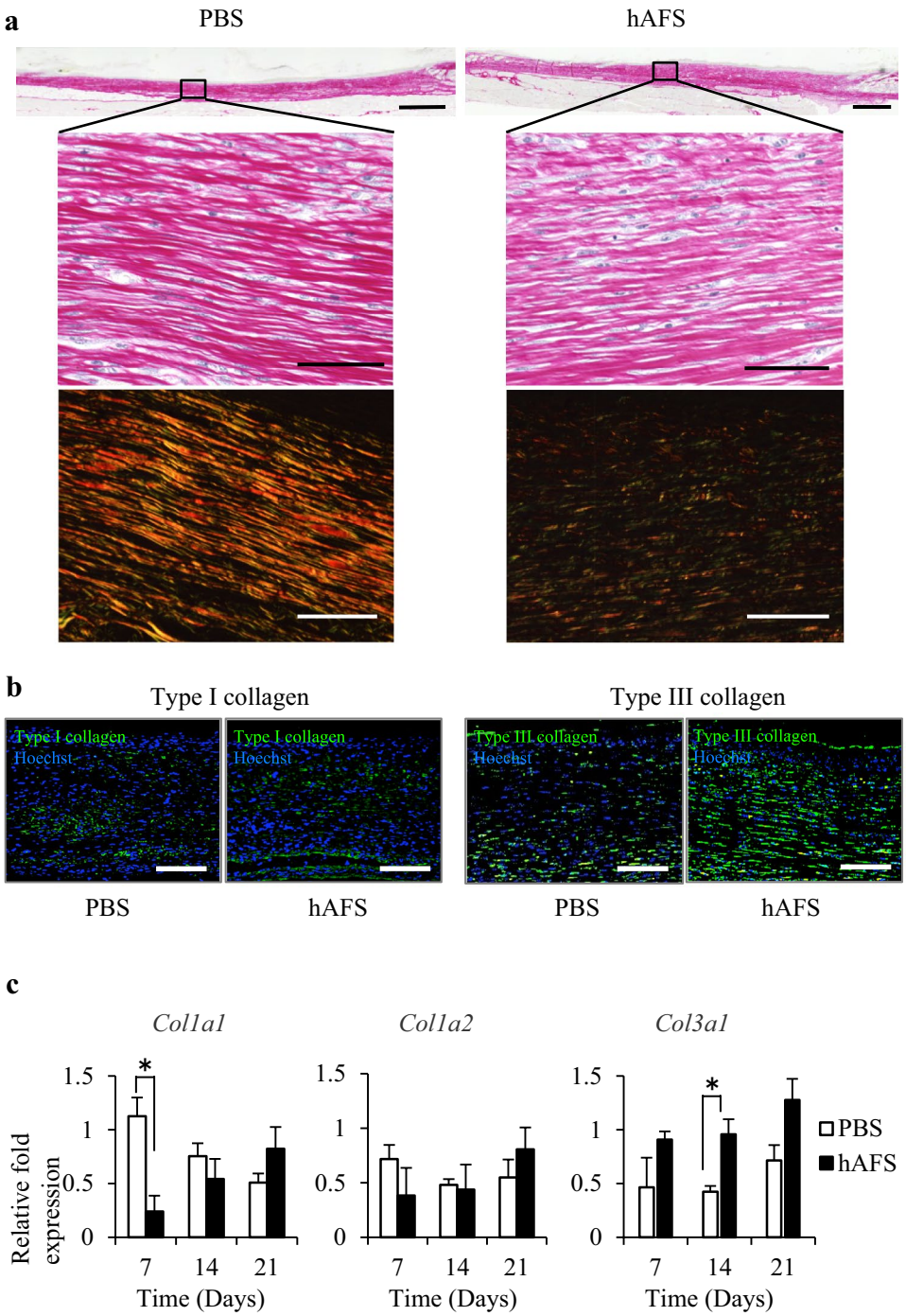

Fig. 4 hAFS treatment altered collagen organization in the regenerated tissues 21 days after treatment. **a** Representative images of regenerated tissue stained with Picrosirius red using optical (upper) and polarized light microscopy (lower) at day 21. The alignment of type I collagen (yellow and red) and type III collagen (green) was observed by polarized microscopy (lower). Scale bars = 1 mm (upper), 50 µm (lower). **b** Representative immunofluorescent stains of the regenerated tissue at day 21 using antibodies against type I (left) and type III (right) collagen, followed by Hoechst staining. Scale bars = 100 µm. **c** Quantitative real-time PCR of *Col1a1, Col1a2, and Col3a1* expression levels at days 7, 14 and 21 ($n = 3$). Images are representative of 3 independent experiments. Results are presented as means ± SD. $^*P < 0.05$ compared to control

immunohistochemical analysis to determine the localization of human-derived cells using anti-human mitochondria antibodies (Supplemental Fig. 1). In accordance with the results of PKH26 analysis, human-derived cells could be observed at days 1, 4, 7, and 14. However, no labeled cells could be detected in the wound at day 21. These results suggested that hAFS transplanted into the epidermis might accelerate wound closure via enhancement of re-epithelialization through direct differentiation into epidermal cells (such as keratinocytes) and through paracrine mechanisms. In contrast, hAFS in the dermis might alter collagen organization by paracrine signaling, not by direct differentiation into dermal cells.

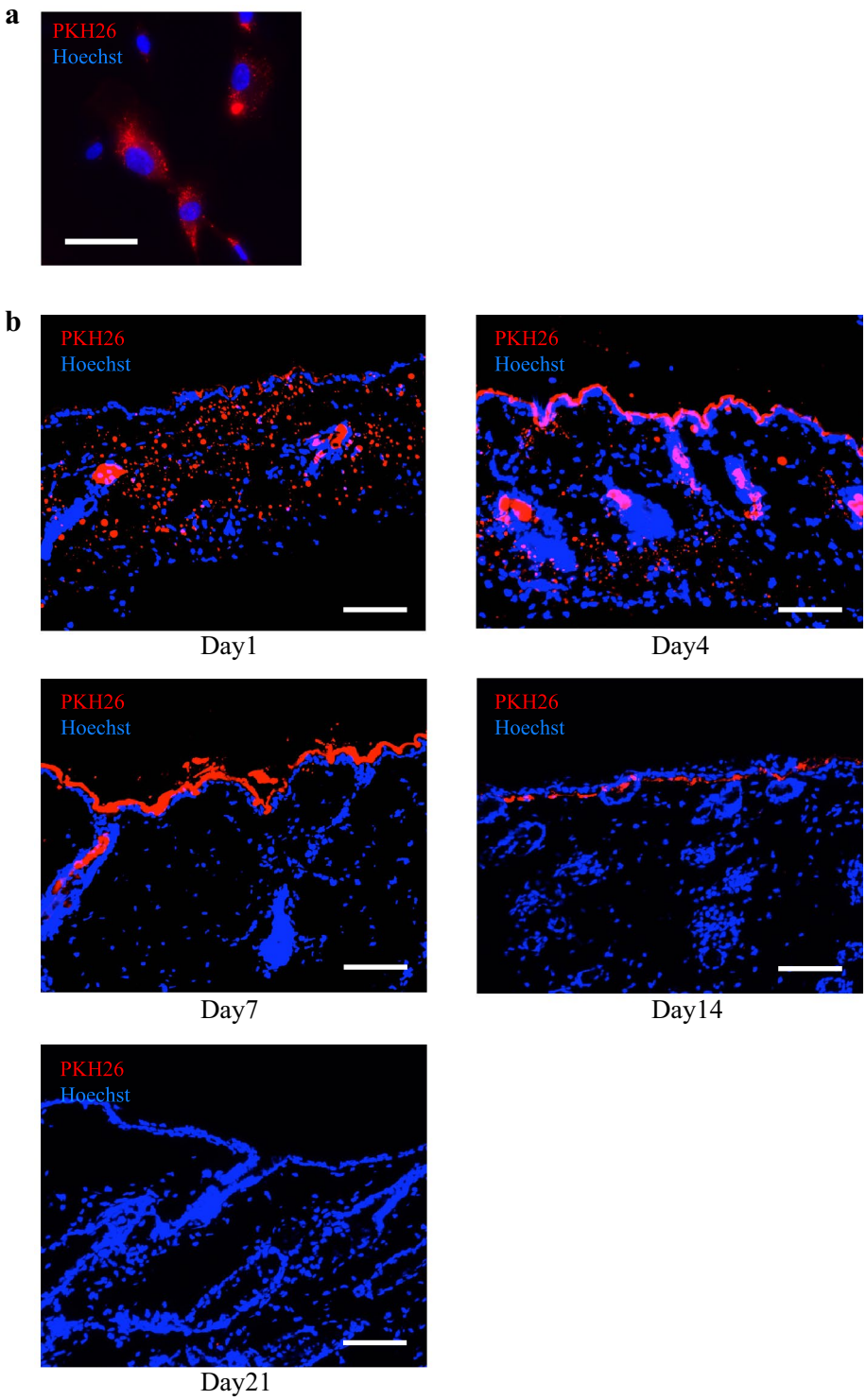

Fig. 5 Engraftment of hAFS in wound. **a** Representative images of hAFS labeled with PKH-26 in vitro (red). Cells were stained with Hoechst. Scale bar = 50 μm. **b** Immunofluorescent and Hoechst staining of the cutaneous tissues 1, 7, 14 and 21 days after injection of hAFS labeled with PKH-26. Scale bar = 200 μm. Images are representative of 3 independent experiments

Discussion

In the present study, we demonstrated that hAFS have a unique potential to accelerate cutaneous wound healing with less fibrotic scarring, thereby resembling fetal wound healing.

MSCs have demonstrated an ability to modulate the wound environment to accelerate wound closure [9–11]. In our study, hAFS treatment accelerated cutaneous wound closure by enhancing re-epithelialization for up to 14 days. Moreover, hAFS, which could differentiate into an ectodermal lineage, were engrafted in the epidermis during this

period. In the literature, there is considerable debate over the mechanisms by which MSCs promote cutaneous wound healing. Although it appears to be partially due to direct differentiation into epidermal cells and keratinocytes [20], paracrine signaling, such as the release of trophic factors that promote angiogenesis, immunomodulation, and recruitment of endogenous tissue stem cells, has been suggested as possible mechanism underlying the effects of MSCs in wound healing [9, 11, 21]. Among MSCs, hAFS and their conditioned medium have been reported to promote wound closure by direct differentiation into keratinocytes and through paracrine signaling via the TGF-β/SMAD2 pathway [20, 22]. We suggest that both direct differentiation and paracrine effects contribute to wound closure in our study [20, 22].

Murine full-thickness wounds close through re-epithelialization and through α-SMA-positive myofibroblast-driven contraction in granulation tissue. In granulation tissue, fibroblasts constitute the main cell population. They are present in the dermis, proliferate rapidly, and migrate to wound sites and differentiate into myofibroblast due to stimulation by growth factors such as transforming growth factor-β in the wound. The continued presence and activation of myofibroblasts during wound regeneration induce fibrotic scarring [1, 2, 4, 5, 7, 19, 23]. In the present study, we found that hAFS treatment suppressed α-SMA-positive myofibroblast expression at the transcriptional level in the dermis, implying that hAFS improves the quality of ECM remodeling and accelerates wound closure independent of wound contraction by regulating fibroblast differentiation into myofibroblast that is the major determinant for fibrotic scarring in the regenerating tissue.

Few studies have focused on the anti-fibrotic effect of MSCs on ECM remodeling during wound healing. Their potential for reduced fibrotic scarring is less well established in vivo, as a result of sometimes conflicting findings [21, 24–32]. To the best of our knowledge, this is the first study focusing on the anti-fibrotic effect of hAFS treatment on ECM remodeling during wound healing. We found that hAFS treatment had anti-fibrotic effects in the dermis, thereby resembling fetal wound healing. Healing was characterized by higher expression of type III collagen at the transcriptional level, which was followed by a significant decrease of α-SMA-positive myofibroblasts. There are phenotypic differences between the collagen contents in fetal and adult wounds. In adults, after exposure to inflammatory mediators in wounds, dermal fibroblasts differentiate into myofibroblasts that express excessive type I collagen, leading to scar formation. On the other hand, fetal dermal fibroblasts before 18 days of gestation in mice and 24 weeks of gestations in humans synthesize more type III collagen, leading to scar-free fetal wound healing [2–6]. Our data suggest that hAFS cells regulate fibroblast differentiation resulting in improved ECM remodeling during wound healing. This might be achieved by converting dermal fibroblasts into fetal-like fibroblasts (not to myofibroblast of adult character), resulting in less fibrotic scarring.

MSCs possess a number of trophic functions that modulate fibrotic scarring [29]. In the present study, paracrine factors secreted from hAFS transiently engrafted in the dermis during the inflammatory phase (i.e., at days 1 and 4) might play a pivotal role in regulating fibroblast phenotype. Notably, IL-10 and PGE_2, both of which were observed in the hAFS secretome in our study, are potent mediators that inhibit inflammatory and fibrotic responses by regulating fibroblast phenotype during wound healing [33–36]. Although further investigation is needed to elucidate the detailed mechanisms by which the hAFS secretome regulates fibroblast differentiation and thereby enhances ECM remodeling during wound healing, our results suggest that hAFS regulate fibroblast differentiation and exert anti-fibrotic effects on wound healing through a paracrine mechanism.

In vivo therapeutic potential of MSCs depends on its source [37]. The limitation of the study was that we did not compare the anti-fibrotic effect of hAFS on cutaneous wound healing with other MSCs derived from bone marrow (BM) and adipose tissue. However, in the present study, we directly compared IL-10 and PGE2 secretions derived from hAFS and BM-MSCs under the same conditions in vitro (Supplemental Fig. 2). Interestingly, IL-10 concentration was comparable between hAFS group and BM-MSC group. However, PGE 2 was significantly higher in the BM-MSC group cultured over 24 h compared to hAFS. These results indicated the difference of immune responses between hAFS and BM-MSCs, suggesting that we need to compare the anti-fibrotic effect of hAFS in vivo with other MSCs. Doi et al. recently described that the therapeutic effect of MSCs derived from umbilical cord blood and Wharton's jelly on cutaneous wound healing were comparable [38]. As to hAFS, we would like to address this question using in vivo studies in future investigations.

Amniotic fluid contains cells derived from developing fetal tissues, including fetal skin [13]. These cells might promote cutaneous wound healing because the factors responsible for scarless fetal wound healing have been attributed to the developing fetal tissue itself [2, 3, 6]. Therefore, it is reasonable that hAFS could have significant anti-fibrotic potential for cutaneous wound healing. In other words, our findings suggest that hAFS could contribute to fetal scarless wound healing as suggested by recent studies [3, 8].

hAFS cells offer intriguing potentials for autologous stem cell treatment for a variety of complications in neonates, including congenital abnormalities and preterm birth. To prepare an adequate amount of autologous hAFS for these neonates, only a small amount of amniotic fluid cells collected by amniocentesis is required, with minimal invasive

risk for the patient. hAFS have an anti-fibrotic potential for treatment of intractable perinatal diseases and can target various organs, including lung [39, 40], kidney [41–44] and liver [45] as well as cutaneous wounds. Thus, anti-fibrotic treatment by hAFS could be a promising autologous stem cell therapy for intractable perinatal diseases.

Conclusion

Our study provides evidence that hAFS have a unique potential to accelerate cutaneous wound healing with reduced fibrotic scarring. Anti-fibrotic treatment using hAFS could be a promising autologous stem cell therapy for intractable perinatal diseases.

Acknowledgements This work was supported by JSPS Grant-in-Aid for Scientific Research (C) Grant number JP15K09724 (https://www.jsps.go.jp/english/e-grants/), JSPS Grant-in-Aid for Scientific Research (B) Grant number 17H04236 (https://www.jsps.go.jp/english/e-grants/), JSPS Grant-in-Aid for Challenging Exploratory Research Grant number JP16K15536 (https://www.jsps.go.jp/english/e-grants/), JAOG Ogyaa Donation Foundation (http://www.ogyaa.or.jp/), Japan Spina Bifida and Hydrocephalus Research Foundation (http://www.jikeikai-group.or.jp/jsatoshi/), Keio Gijuku Academic Development Funds research funding (individual research) (http://www.rcp.keio.ac.jp/ora/jukunai/gakushin.html#two), and Kawano Masanori Memorial Public Interest Incorporated Foundation for Promotion of Pediatrics (https://kawanozaidan.or.jp/c).

Author contributions MF, DO, HM, SS, NA, MS, YK, KK, and MT conceived and designed the experiments. MF, DO, YA, and TO performed the experiments. MF, DO, HM, YA, TO, SS, NA, MS, TM, KM, YK, KK, and MT analyzed the data. SS and MS contributed reagents/materials/analytic tools. MF, DO, HM, and MT wrote the paper.

Compliance with ethical standards

Conflict of interest The authors have no conflicts of interest to declare.

References

1. Singer AJ, Clark RA. Cutaneous wound healing. N Engl J Med. 1999;341(10):738–746. https://doi.org/10.1056/NEJM199909023411006.
2. Kishi K, Okabe K, Shimizu R, Kubota Y. Fetal skin possesses the ability to regenerate completely: complete regeneration of skin. Keio J Med. 2012;61(4):101–8. https://doi.org/10.2302/kjm.2011-0002-IR.
3. Hu MS, Maan ZN, Wu JC, Rennert RC, Hong WX, Lai TS, et al. Tissue engineering and regenerative repair in wound healing. Ann Biomed Eng. 2014;42(7):1494–507. https://doi.org/10.1007/s10439-014-1010-z.
4. Larson BJ, Longaker MT, Lorenz HP. Scarless fetal wound healing: a basic science review. Plast Reconstr Surg. 2010;126(4):1172–80. https://doi.org/10.1097/PRS.0b013e3181eae781.
5. Lo DD, Zimmermann AS, Nauta A, Longaker MT, Lorenz HP. Scarless fetal skin wound healing update. Birth Defects Res C Embryo Today. 2012;96(3):237–47. https://doi.org/10.1002/bdrc.21018.
6. Leung A, Crombleholme TM, Keswani SG. Fetal wound healing: implications for minimal scar formation. Curr Opin Pediatr. 2012;24(3):371–8. https://doi.org/10.1097/MOP.0b013e3283535790.
7. Friedman SL, Sheppard D, Duffield JS, Violette S. Therapy for fibrotic diseases: nearing the starting line. Sci Transl Med. 2013;5(167):167 sr1. https://doi.org/10.1126/scitranslmed.3004700.
8. Klein JD, Turner CG, Steigman SA, Ahmed A, Zurakowski D, Eriksson E, et al. Amniotic mesenchymal stem cells enhance normal fetal wound healing. Stem Cells Dev. 2011;20(6):969–76. https://doi.org/10.1089/scd.2010.0379.
9. Jackson WM, Nesti LJ, Tuan RS. Concise review: clinical translation of wound healing therapies based on mesenchymal stem cells. Stem Cells Transl Med. 2012;1(1):44–50. https://doi.org/10.5966/sctm.2011-0024.
10. Li M, Zhao Y, Hao H, Han W, Fu X. Mesenchymal stem cell-based therapy for nonhealing wounds: today and tomorrow. Wound Repair Regen. 2015;23(4):465–82. https://doi.org/10.1111/wrr.12304.
11. Lee DE, Ayoub N, Agrawal DK. Mesenchymal stem cells and cutaneous wound healing: novel methods to increase cell delivery and therapeutic efficacy. Stem Cell Res Ther. 2016;7:37. https://doi.org/10.1186/s13287-016-0303-6.
12. De Coppi P, Bartsch G Jr, Siddiqui MM, Xu T, Santos CC, Perin L, et al. Isolation of amniotic stem cell lines with potential for therapy. Nat Biotechnol. 2007;25(1):100–6. https://doi.org/10.1038/nbt1274.
13. Loukogeorgakis SP, De Coppi P. Amniotic fluid stem cells: the known, the unknown and potential regenerative medicine applications. Stem Cells. 2016. https://doi.org/10.1002/stem.2553.
14. Roubelakis MG, Bitsika V, Zagoura D, Trohatou O, Pappa KI, Makridakis M, et al. In vitro and in vivo properties of distinct populations of amniotic fluid mesenchymal progenitor cells. J Cell Mol Med. 2011;15(9):1896–913. https://doi.org/10.1111/j.1582-4934.2010.01180.x.
15. Hattori N, Mochizuki S, Kishi K, Nakajima T, Takaishi H, D'Armiento J, et al. MMP-13 plays a role in keratinocyte migration, angiogenesis, and contraction in mouse skin wound healing. Am J Pathol. 2009;175(2):533–46. https://doi.org/10.2353/ajpath.2009.081080.
16. Dominici M, Le Blanc K, Mueller I, Slaper-Cortenbach I, Marini F, Krause D, et al. Minimal criteria for defining multipotent mesenchymal stromal cells. The International Society for Cellular Therapy position statement. Cytotherapy. 2006;8(4):315–7. https://doi.org/10.1080/14653240600855905.
17. Perin L, Sedrakyan S, Da Sacco S, De Filippo R. Characterization of human amniotic fluid stem cells and their pluripotential capability. Methods Cell Biol. 2008;86:85–99. https://doi.org/10.1016/s0091-679x(08)00005-8.
18. Yan ZJ, Hu YQ, Zhang HT, Zhang P, Xiao ZY, Sun XL, et al. Comparison of the neural differentiation potential of human mesenchymal stem cells from amniotic fluid and adult bone marrow. Cell Mol Neurobiol. 2013;33(4):465–475. https://doi.org/10.1007/s10571-013-9922-y.
19. Gurtner GC, Werner S, Barrandon Y, Longaker MT. Wound repair and regeneration. Nature. 2008;453(7193):314–321. https://doi.org/10.1038/nature07039.
20. Sun Q, Li F, Li H, Chen RH, Gu YZ, Chen Y, et al. Amniotic fluid stem cells provide considerable advantages in epidermal regeneration: B7H4 creates a moderate inflammation microenvironment to promote wound repair. Sci Rep. 2015;5:11560. https://doi.org/10.1038/srep11560.

21. Wu Y, Chen L, Scott PG, Tredget EE. Mesenchymal stem cells enhance wound healing through differentiation and angiogenesis. Stem Cells. 2007;25(10):2648–2659. https://doi.org/10.1634/stemcells.2007-0226.
22. Yoon BS, Moon JH, Jun EK, Kim J, Maeng I, Kim JS, et al. Secretory profiles and wound healing effects of human amniotic fluid-derived mesenchymal stem cells. Stem Cells Dev. 2010;19(6):887–902. https://doi.org/10.1089/scd.2009.0138.
23. Sakai S, Sato K, Tabata Y, Kishi K. Local release of pioglitazone (a peroxisome proliferator-activated receptor gamma agonist) accelerates proliferation and remodeling phases of wound healing. Wound Repair Regen. 2016;24(1):57–64. https://doi.org/10.1111/wrr.12376.
24. Qi Y, Jiang D, Sindrilaru A, Stegemann A, Schatz S, Treiber N, et al. TSG-6 released from intradermally injected mesenchymal stem cells accelerates wound healing and reduces tissue fibrosis in murine full-thickness skin wounds. J Invest Dermatol. 2014;134(2):526–37. https://doi.org/10.1038/jid.2013.328.
25. Wu Y, Huang S, Enhe J, Ma K, Yang S, Sun T, et al. Bone marrow-derived mesenchymal stem cell attenuates skin fibrosis development in mice. Int Wound J. 2014;11(6):701–10. https://doi.org/10.1111/iwj.12034.
26. Huang S, Wu Y, Gao D, Fu X. Paracrine action of mesenchymal stromal cells delivered by microspheres contributes to cutaneous wound healing and prevents scar formation in mice. Cytotherapy. 2015;17(7):922–31. https://doi.org/10.1016/j.jcyt.2015.03.690.
27. McFarlin K, Gao X, Liu YB, Dulchavsky DS, Kwon D, Arbab AS, et al. Bone marrow-derived mesenchymal stromal cells accelerate wound healing in the rat. Wound Repair Regen. 2006;14(4):471–478. https://doi.org/10.1111/j.1743-6109.2006.00153.x.
28. Chen L, Xu Y, Zhao J, Zhang Z, Yang R, Xie J, et al. Conditioned medium from hypoxic bone marrow-derived mesenchymal stem cells enhances wound healing in mice. PLoS One. 2014;9(4):e96161. https://doi.org/10.1371/journal.pone.0096161.
29. Li Q, Zhang C, Fu X. Will stem cells bring hope to pathological skin scar treatment? Cytotherapy. 2016;18(8):943–56. https://doi.org/10.1016/j.jcyt.2016.05.008.
30. Kwon DS, Gao X, Liu YB, Dulchavsky DS, Danyluk AL, Bansal M, et al. Treatment with bone marrow-derived stromal cells accelerates wound healing in diabetic rats. Int Wound J. 2008;5(3):453–63. https://doi.org/10.1111/j.1742-481X.2007.00408.x.
31. Ding J, Ma Z, Shankowsky HA, Medina A, Tredget EE. Deep dermal fibroblast profibrotic characteristics are enhanced by bone marrow-derived mesenchymal stem cells. Wound Repair Regen. 2013;21(3):448–55. https://doi.org/10.1111/wrr.12046.
32. Fu X, Li H. Mesenchymal stem cells and skin wound repair and regeneration: possibilities and questions. Cell Tissue Res. 2009;335(2):317–21. https://doi.org/10.1007/s00441-008-0724-3.
33. Seo SY, Han SI, Bae CS, Cho H, Lim SC. Effect of 15-hydroxyprostaglandin dehydrogenase inhibitor on wound healing. Prostaglandins Leukot Essent Fatty Acids. 2015;97:35–41. https://doi.org/10.1016/j.plefa.2015.03.005.
34. Kieran I, Knock A, Bush J, So K, Metcalfe A, Hobson R, et al. Interleukin-10 reduces scar formation in both animal and human cutaneous wounds: results of two preclinical and phase II randomized control studies. Wound Repair Regen. 2013;21(3):428–36. https://doi.org/10.1111/wrr.12043.
35. Balaji S, Wang X, King A, Le LD, Bhattacharya SS, Moles CM, et al. Interleukin-10-mediated regenerative postnatal tissue repair is dependent on regulation of hyaluronan metabolism via fibroblast-specific STAT3 signaling. FASEB J. 2017;31(3):868–81. https://doi.org/10.1096/fj.201600856R.
36. Sandulache VC, Parekh A, Li-Korotky HS, Dohar JE, Hebda PA. Prostaglandin E2 differentially modulates human fetal and adult dermal fibroblast migration and contraction: implication for wound healing. Wound Repair Regen. 2006;14(5):633–643. https://doi.org/10.1111/j.1743-6109.2006.00156.x.
37. Bortolotti F, Ukovich L, Razban V, Martinelli V, Ruozi G, Pelos B, et al. In vivo therapeutic potential of mesenchymal stromal cells depends on the source and the isolation procedure. Stem Cell Rep. 2015;4(3):332–9. https://doi.org/10.1016/j.stemcr.2015.01.001.
38. Doi H, Kitajima Y, Luo L, Yan C, Tateishi S, Ono Y, et al. Potency of umbilical cord blood- and Wharton's jelly-derived mesenchymal stem cells for scarless wound healing. Sci Rep. 2016;6:18844. https://doi.org/10.1038/srep18844.
39. Wen ST, Chen W, Chen HL, Lai CW, Yen CC, Lee KH, et al. Amniotic fluid stem cells from EGFP transgenic mice attenuate hyperoxia-induced acute lung injury. PLoS One. 2013;8(9):e75383. https://doi.org/10.1371/journal.pone.0075383.
40. Garcia O, Carraro G, Turcatel G, Hall M, Sedrakyan S, Roche T, et al. Amniotic fluid stem cells inhibit the progression of bleomycin-induced pulmonary fibrosis via CCL2 modulation in bronchoalveolar lavage. PLoS One. 2013;8(8):e71679. https://doi.org/10.1371/journal.pone.0071679.
41. Baulier E, Favreau F, Le Corf A, Jayle C, Schneider F, Goujon JM, et al. Amniotic fluid-derived mesenchymal stem cells prevent fibrosis and preserve renal function in a preclinical porcine model of kidney transplantation. Stem Cells Transl Med. 2014;3(7):809–20. https://doi.org/10.5966/sctm.2013-0186.
42. Sedrakyan S, Da Sacco S, Milanesi A, Shiri L, Petrosyan A, Varimezova R, et al. Injection of amniotic fluid stem cells delays progression of renal fibrosis. J Am Soc Nephrol. 2012;23(4):661–73. https://doi.org/10.1681/ASN.2011030243.
43. Sun D, Bu L, Liu C, Yin Z, Zhou X, Li X, et al. Therapeutic effects of human amniotic fluid-derived stem cells on renal interstitial fibrosis in a murine model of unilateral ureteral obstruction. PLoS One. 2013;8(5):e65042. https://doi.org/10.1371/journal.pone.0065042.
44. Monteiro Carvalho Mori da Cunha MG, Zia S, Oliveira Arcolino F, Carlon MS, Beckmann DV, Pippi NL, et al. Amniotic fluid derived stem cells with a renal progenitor phenotype inhibit interstitial fibrosis in renal ischemia and reperfusion injury in rats. PLoS One. 2015;10(8):e0136145. https://doi.org/10.1371/journal.pone.0136145.
45. Peng SY, Chou CJ, Cheng PJ, Ko IC, Kao YJ, Chen YH, et al. Therapeutic potential of amniotic-fluid-derived stem cells on liver fibrosis model in mice. Taiwan J Obstet Gynecol. 2014;53(2):151–7. https://doi.org/10.1016/j.tjog.2014.04.005.